# Exploratory CFD aeroacoustic study of a ducted fan with bioinspired (biomimetic) blades

URANS $k$–$\omega$ SST flow (sliding-mesh AMI) and tonal noise via the Ffowcs-Williams & Hawkings analogy

Polytechnia project — OpenFOAM v2506 & libAcoustics

June 29, 2026

**Abstract**

This report presents an **exploratory numerical study** of the aeroacoustic signature of a ducted desk fan whose blades carry trailing-edge serrations (biomimicry inspired by owl feathers [1]). The workflow chains an unsteady flow simulation (**URANS** $k$–$\omega$ **SST**, sliding-mesh AMI, $\approx 1.95$ M cells) with the extraction of the radiated noise using the **Ffowcs-Williams & Hawkings analogy** (Farassat 1A formulation, `libAcoustics`) at four observers placed at 1 m. We detail the methodology, the mesh, the flow field (jet, wake, vortices, blade loading), the aerodynamic performance and the acoustic analysis (signals, spectra, levels). Results are provided **on an exploratory basis**: convergence checks (mesh and time-step independence), boundary-layer resolution, and quantification of the biomimetic effect remain to be carried out and are explicitly listed.

## Contents

# 1 Objective and context

The goal is to set up and run a **CFD–FW-H workflow** to characterise the noise, in particular its **tonal** component (the blade-passing frequency, BPF, and its harmonics). The acoustic methodology follows bioinspired-noise studies [1]. **The blade geometry is not modified**: the blades studied are already biomimetic (Figure 1). This work does *not* aim to demonstrate an acoustic benefit of the biomimicry (which would require a smooth reference rotor, §8), but to establish a first numerical characterisation.

# 2 Geometry

A **5-blade** impeller ($R \approx 69\,\text{mm}$, diameter 138 mm), a venturi-shaped shroud (casing), a central hub/motor and three support arms. The blades feature **trailing-edge serrations** (Figure 1).

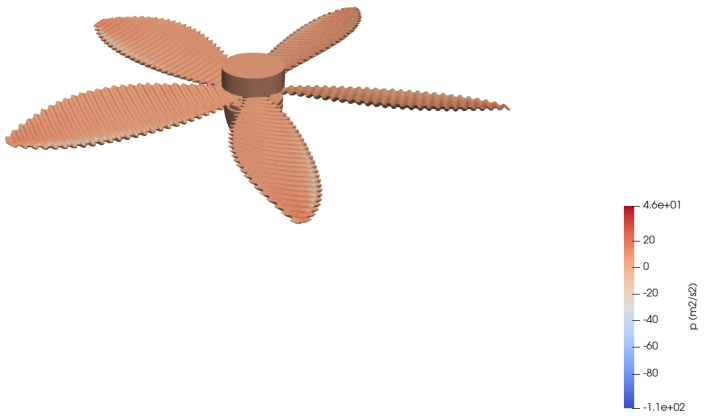


Figure 1: 5-blade impeller coloured by kinematic pressure. The **serrated trailing edges** (biomimetic features) are clearly visible.

# 3 Methodology

## 3.1 Principle

Tonal noise originates from the **unsteady force exerted by the blades on the fluid** (dipole source). The chain is: CAD geometry → AMI mesh → URANS $k$-$\omega$ SST → FW-H → observers.

## 3.2 Why the FW-H analogy?

Two reasons: (i) the domain is only ∼0.3 m across, so the microphones (1 m) lie outside it; (ii) the incompressible solver does not carry acoustic waves. FW-H records the loading on a surface near the source and propagates the sound *analytically* to the observer.

### 3.3 FW-H surface and observers

The source surface is limited to the `helice` (blades) patch, with `nonUniformSurfaceMotion` (rotating surface), Farassat 1A formulation. This captures the **loading and thickness noise of the blades**. *Assumed limitation* (§8): the fixed surfaces (casing, 3 arms, hub) and the volumetric quadrupole sources are not included; at low Mach number the quadrupoles are usually secondary, but the contribution of the fixed surfaces is not assessed here. Four observers at 1 m: **downstream** (axis), **upstream** (axis), **radial** (side), **diag45**. $c_0 = 343\,\mathrm{m/s}$, $\rho_\infty = 1.2\,\mathrm{kg/m^3}$, reference $20\,\mu\mathrm{Pa}$.

## 4 Mesh

### 4.1 Type chosen

**Hex-dominant** mesh (`snappyHexMesh`): a Cartesian box refined by octree around the STL surfaces, then *snapped* onto the geometry. Chosen for its accuracy at a low cell count, its targeted local refinement, and its native handling of the sliding AMI interface.

### 4.2 Refinement and AMI interface

Background box $0.4 \times 0.4 \times 0.5\,\mathrm{m}$, $40 \times 40 \times 50 \Rightarrow$ base cell 10 mm. A **cyclicAMI** interface (35 660 faces, `createBaffles`) separates the rotating rotor cylinder ($R = 72\,\mathrm{mm}$) from the fixed zone. Figure 2 shows the refinement transition.

| Zone | Level | Cell size |
|---|---|---|
| Blades (helice) | 5 | 0.31 mm |
| Casing, arms | 3 | 1.25 mm |
| Hub/motor | 2 | 2.5 mm |
| Rotor cylinder + wake (vol.) | 2–3 | 1.25–2.5 mm |
| Far field | 0 | 10 mm |

Table 1: Refinement levels.

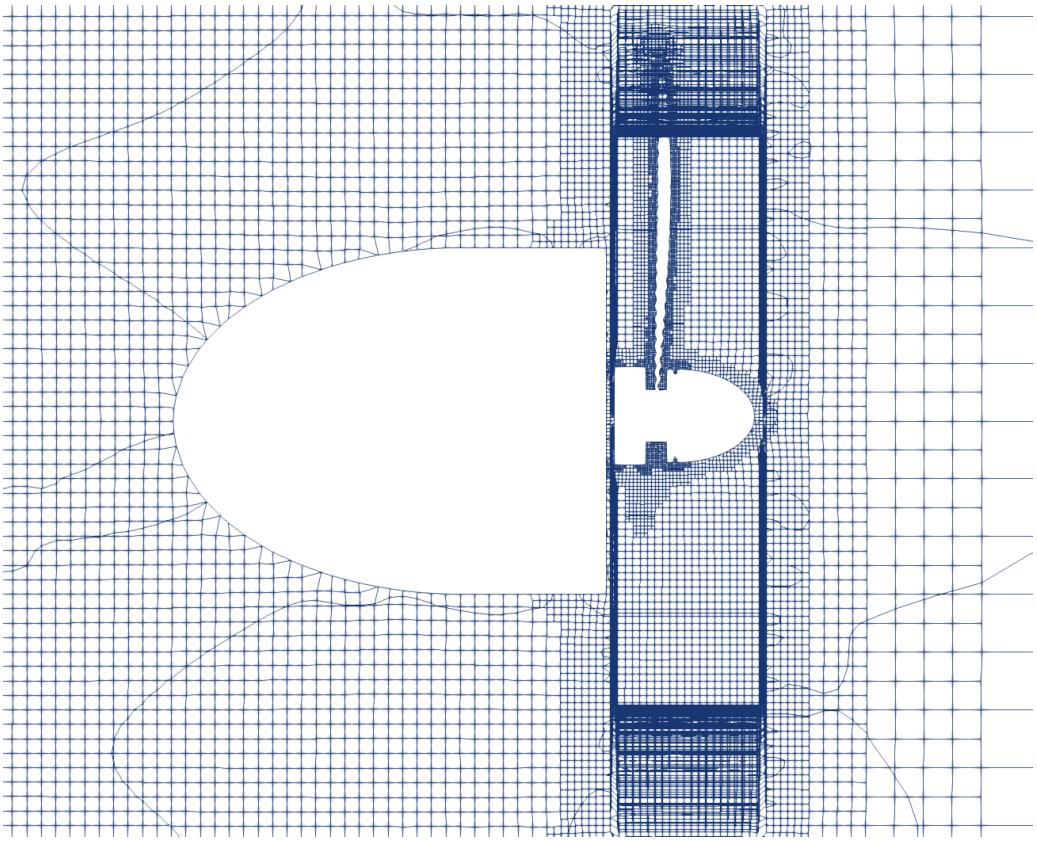

Figure 2: Meridional cut of the mesh: transition from coarse (far field) → fine (rotor) → very fine (blade band / AMI zone).

### 4.3 Mesh quality (exact values)

| | |
|---|---|
| Cells / points | 1 949 584 / 2 205 401 |
| Max aspect ratio | 6.61 |
| Max / avg non-orthogonality | 61.4 / 8.2 |
| Max skewness | 7.25 (12 faces $> 4$) |
| Min / max volume | $3.2 \times 10^{-12}$ / $1.0 \times 10^{-6}\,\mathrm{m}^3$ |
| Cells with determinant $< 0.001$ | 1851 |
| Concave cells (face planes) | 49 827 |
| AMI weights (min / avg / max) | 0.90 / 1.002 / 1.27 |

Table 2: Final mesh quality (`checkMesh`).

**Important note.** Residual concave cells (49 827, i.e. 2.6 %) and 1851 low-determinant cells remain in some geometric transitions (intrinsic to a hex mesh on a curved geometry). The solver runs (with `FOAM_SIGFPE=false` so it does not abort on these cells), but this **does not fix their quality**: their numerical influence — in particular on possible spurious acoustic peaks — **remains to be quantified by a local mesh-sensitivity study**.

### 4.4 Boundary layer and $y^+$: a critical point

The intended prismatic layers (Low-Re, $y^+ \sim 1$) **could not be inserted** on the thin, serrated blades (insufficient coverage): the retained mesh has **no layers**, the first wall cell being the level-5 surface cell. The $y^+$ measured at the last time step is:

| Wall | $y^+_{\min}$ | $y^+_{\mathrm{avg}}$ | $y^+_{\max}$ |
|---|---|---|---|
| helice (blades) | 0.09 | 4.2 | 445 |
| casing | 0.10 | 2.3 | 8.2 |
| motor | 0.26 | 3.4 | 18.9 |
| arms | 0.35 | 6.5 | 15.8 |

Table 3: $y^+$ distribution (no prismatic layers).

The SST model uses automatic wall treatment (blending low-Reynolds / wall functions). The average $y^+$ on the blades ($\approx 4$) falls in the **buffer layer** ($5 < y^+ < 30$), the least well modelled region, and reaches 445 locally (leading edge / blade tip). **Consequently the pressure loading on the blades — hence the dipole noise — must be regarded as preliminary**, pending a mesh with resolved boundary layers.

# 5 Numerical model

- `pimpleFoam` (incompressible, transient), air $\rho = 1.2\,\mathrm{kg/m^3}$, $\nu = 1.5 \times 10^{-5}\,\mathrm{m^2/s}$; $k$–$\omega$ SST turbulence (URANS).
- Solid-body rotation $\omega = 158\,\mathrm{rad/s}$ ($\approx 1509\,\mathrm{rpm}$), startup ramp $0 \to 158\,\mathrm{rad/s}$ over 5 ms.
- BPF $= Z\,n = 5 \times 25.15 = 126\,\mathrm{Hz}$.

**Two phases.** Phase 1 (establish): adaptive time step, Co $\leq 5$; in practice a fine cell limited $\Delta t \approx 3.7 \times 10^{-5}\,\mathrm{s}$. Phase 2 (acoustic): **fixed** time step $\Delta t = 3.5 \times 10^{-5}\,\mathrm{s}$, FW-H enabled (the FFT requires uniform sampling). *Limitation*: time-step independence (and the relatively high Co in phase 1) was not verified with a second $\Delta t$.

# 6 Aerodynamic results

## 6.1 Established regime and loads

Figure 3 shows thrust and torque: a startup transient peak followed by stabilisation. The regime is **quasi-periodic established** after $\approx 4.75$ revolutions (thrust variation $< 1\,\%$ per rev). *Limitation*: a revolution-to-revolution repeatability study over more revolutions would strengthen this statement.

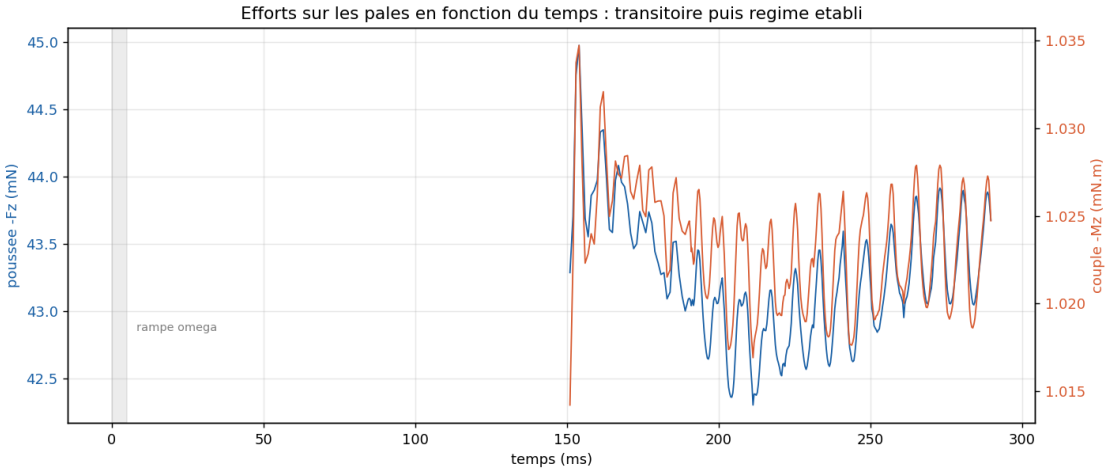


Figure 3: Thrust ($-F_z$) and torque ($-M_z$) versus time: startup transient then established regime. (Axis labels in French in the source figure.)

| | |
|---|---|
| Axial thrust | 43.3 mN |
| Torque | 1.02 mN m |
| Aerodynamic power $C\omega$ | 0.162 W |
| Volume flow rate (downstream plane 60 mm) | $\approx$108 m$^3$/h (30 L/s) |
| Blade-tip speed $\omega R$ | 10.9 m/s |

Table 4: Aerodynamic performance (established regime). *Values not yet compared to a measurement or an analytical correlation.*

## 6.2 Flow fields

The velocity field (Figure 4) shows an **annular jet** and the slow **wake** behind the hub; the vectors (Figure 5) give its direction. The pressure field (Figure 6) shows the suction at the inlet and the overpressure at the outlet. The blade-tip vortices and the helical wake appear on the iso-$Q$ surface (Figure 7), and the imprint of the 5 blades on the downstream cut (Figure 8).

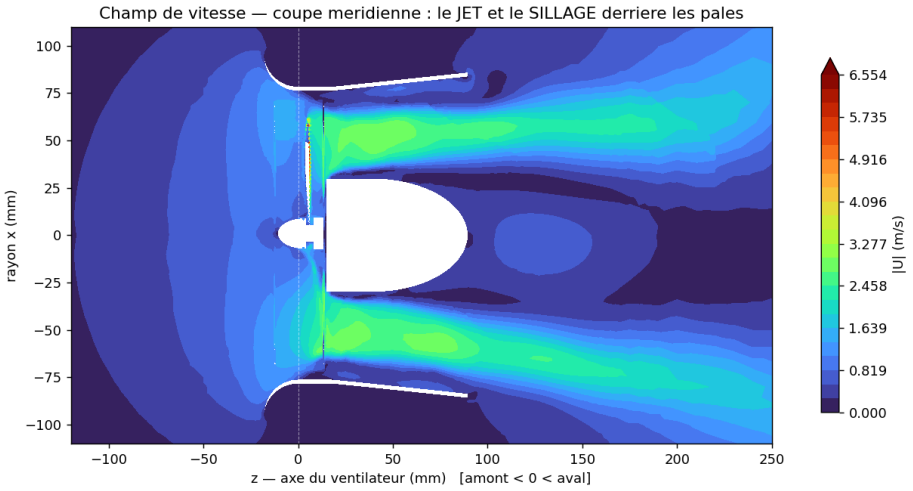


Figure 4: Velocity field, meridional cut: annular jet and hub wake.

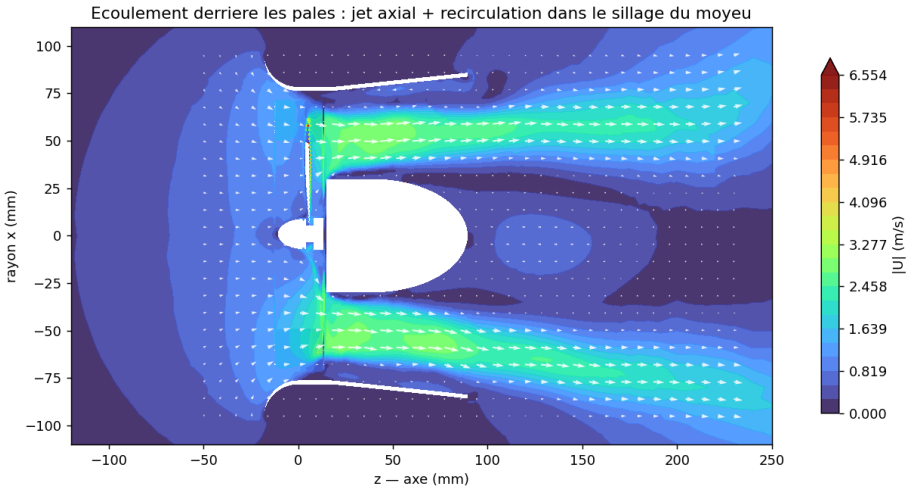


Figure 5: Velocity vectors: axial jet and recirculation in the wake.

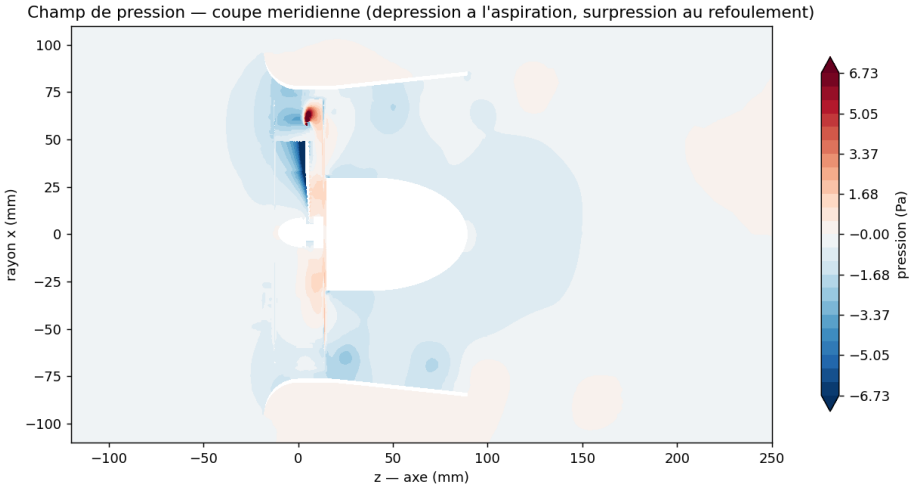


Figure 6: Pressure field (kinematic $\times\rho$), meridional cut.

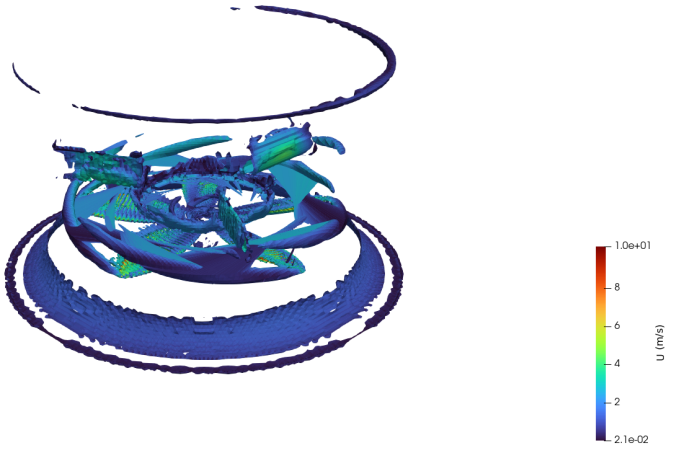


Figure 7: Vortical structures (iso-$Q$) coloured by velocity.

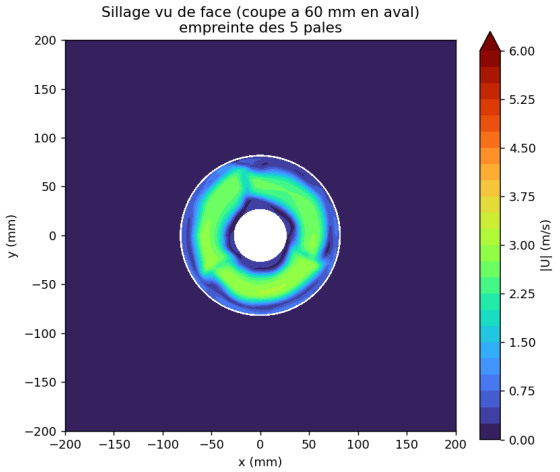


Figure 8: Wake seen face-on (cut 60 mm downstream): imprint of the 5 blades.

These main structures are **qualitatively consistent** with the expected operation of a ducted fan.

# 7 Acoustic analysis

## 7.1 Pressure units

In `pimpleFoam`, the variable $p$ is a **kinematic pressure** ($m^2/s^2$). The conversion to pascals uses $p_{\mathrm{Pa}} = \rho\, p_{\mathrm{kin}}$ with $\rho = 1.2\,\mathrm{kg/m^3}$; SPL levels are computed on $p_{\mathrm{Pa}}$.

## 7.2 Time signal and FFT protocol

FW-H provides $p'(t)$ at the four microphones (Figure 9). The signals show non-zero **mean offsets** (up to $\pm 1.2\,\mathrm{mPa}$): each segment's mean is removed before analysis (the raw signals are not interpreted as pure acoustic pressure). **FFT protocol**: combination of two contiguous recordings (170 ms usable), **Hann** window, $N = 972$ points, $f_s = 5714\,\mathrm{Hz}$ (Nyquist 2857 Hz), **single block** (no Welch averaging), single-sided spectrum, $\Delta f \approx 5.9\,\mathrm{Hz}$, **no A-weighting**. OASPL computed from the RMS signal ($L = 20\log_{10}(p_{\mathrm{rms}}/p_{\mathrm{ref}})$).

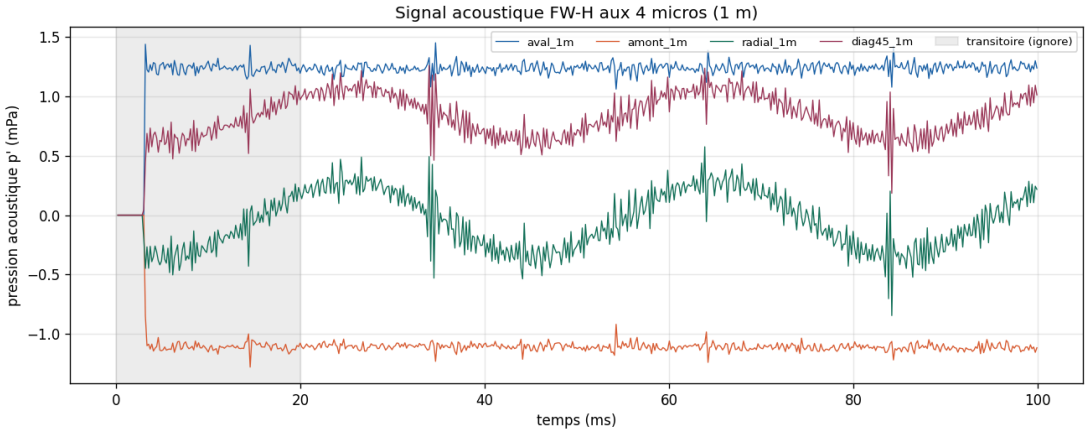


Figure 9: FW-H acoustic signal at the 4 microphones (1 m), raw signals.

## 7.3 Raw and filtered spectra

For transparency, Figure 10 compares the **raw** spectrum (mean removed only) and the **filtered** spectrum (5-point median anti-spike + detrend). Filtering **reduces noise without creating tones**: the BPF and the 25 Hz component are present in both. The median filter could however attenuate possible intermittent fluctuations; ideally these numerical spikes should be fixed at the source (mesh).

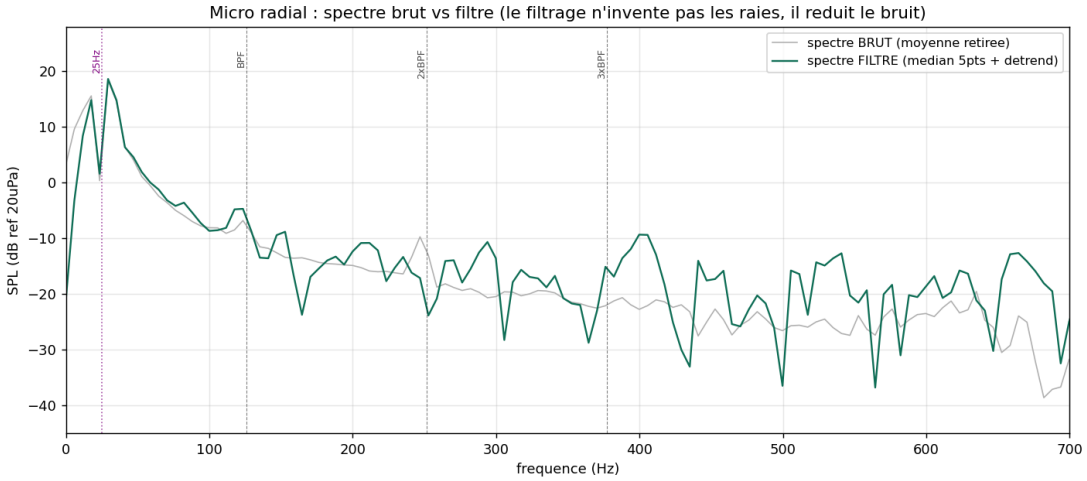


Figure 10: Radial microphone: raw vs filtered spectrum.

## 7.4 SPL spectrum and levels

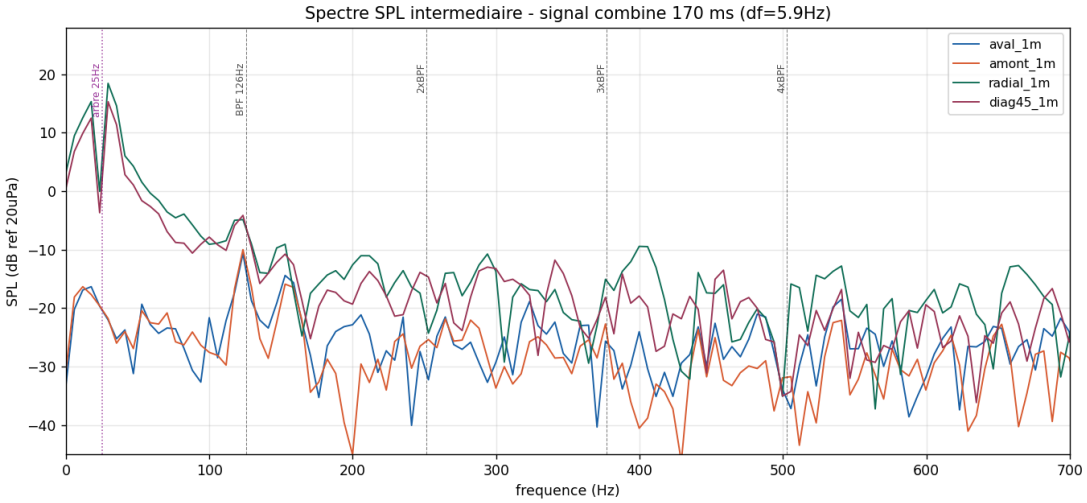


Figure 11: SPL spectrum at the 4 microphones (combined signal 170 ms, $\Delta f = 5.9$ Hz).

| Microphone | 25 Hz (1/rev) | BPF 126 Hz | OASPL |
|---|---|---|---|
| downstream | −20 dB | −11 dB | −1 dB |
| upstream | −20 dB | −10 dB | −3 dB |
| radial | 18 dB | −5 dB | 21 dB |
| diag45 | 15 dB | −4 dB | 18 dB |

Table 5: SPL levels per microphone (dB ref 20 µPa, band 0 Hz to 2857 Hz).

## 7.5 Cautious interpretation

- The four observers indicate **higher levels in the radial and diagonal directions than on the axis** (a full directivity would require a ring of microphones and a polar representation).
- A **significant component appears around the rotation frequency** (25 Hz). Its robustness must be confirmed on a longer recording and after checking the influence of the startup transient: at 170 ms only ∼4–5 periods at 25 Hz are captured.

- The **BPF** (126 Hz) tone is consistent with $5 \times 25.15$ Hz. Its confirmation would require an **engine-order** analysis, the presence of harmonics (2BPF, 3BPF) and stability across several windows.
- Modest absolute levels ($\sim 20$ dB): see §8.

# 8 Limitations and validations to be carried out

1. **Mesh independence not established.** A 1.95M-cell mesh was *retained*, but not *validated*: at least 3 meshes should be compared on thrust, flow rate, torque and BPF amplitude.
2. **Boundary layer not resolved** (§4.4): no prismatic layers, average $y^+ \approx 4$ and max 445 on the blades $\Rightarrow$ preliminary surface loading.
3. **Time-step independence not verified**: a second $\Delta t$ would be needed to prove the stability of the BPF peak.
4. **URANS**: mainly represents the coherent, tonal components, but does not reliably resolve the **broadband turbulent noise** $\Rightarrow$ underestimated absolute levels.
5. **FW-H surface** limited to the blades (casing, arms, hub, quadrupoles excluded, §3.3).
6. **Recording duration** short ($\Delta f \approx 5.9$ Hz): the 25 Hz peak to be confirmed.
7. **Biomimicry not quantified**: without a smooth reference rotor (same conditions), and since the serrations act mainly on the broadband (not resolved in URANS), the proper acoustic effect of the serrations cannot be measured here. The obtained spectrum is the *signature* of the biomimetic fan, not the *measure of the effect* of the serrations.

**Priority improvement plan.** (1) mesh and time-step independence study; (2) mesh with boundary layers and controlled $y^+$; (3) longer recording + reproducible FFT protocol; (4) smooth reference rotor (same conditions) to compare the tonal components; (5) **LES/IDDES** approach for the broadband, and comparison with a measurement (flow rate, thrust, noise).

# 9 Conclusion

The **CFD–FW-H workflow was executed** on the studied geometry and produces aerodynamic results (jet, wake, vortices, loading) and acoustic results (spectra at the 4 observers) **usable on an exploratory basis**. The flow structures are qualitatively consistent with a ducted fan. The predicted noise shows a dominant component around 25 Hz (to be confirmed) and an identifiable BPF tone (126 Hz), with higher levels laterally. **The defensible conclusion is**: *the CFD–FW-H workflow is operational and provides a first characterisation of the tonal components and their dependence on observation direction; the proper acoustic impact of the serrations remains to be quantified (smooth reference rotor, mesh and time-step validation, longer recording, an approach suited to broadband noise).*

# References


[1] Z. Wei, S. Wang, S. Farris, N. Chennuri, N. Wang, S. Shinsato, K. Demir, M. Horii, G. X. Gu, *Towards silent and efficient flight by combining bioinspired owl feather serrations with cicada wing geometry*, Nature Communications, 2024. (Gu Research Group, University of California, Berkeley.)

[2] J. E. Ffowcs Williams, D. L. Hawkings, *Sound generation by turbulence and surfaces in arbitrary motion*, Phil. Trans. R. Soc. A, 264, 1969.

[3] F. Farassat, *Derivation of Formulations 1 and 1A of Farassat*, NASA/TM-2007-214853, 2007.

[4] F. R. Menter, *Two-equation eddy-viscosity turbulence models for engineering applications*, AIAA Journal, 32(8), 1994.

[5] *libAcoustics* (UNICFD lab), FW-H library for OpenFOAM.

[6] OpenFOAM v2506, `cyclicAMI` / `snappyHexMesh` User Guide, OpenCFD/ESI.

[7] W. Neise, *Review of fan noise generation mechanisms and control methods*, Fan Noise Symposium, 1992.

[8] T. P. Chong et al., *On the noise reduction of trailing edge serrations*, J. Sound Vib.